Research Article

Dennis Dolkens, Hans Kuiper* and Victor Villalba Corbacho

The deployable telescope: a cutting-edge solution for high spatial and temporal resolved Earth observation

https://doi.org/10.1515/aot-2018-0043
Received August 20, 2018; accepted October 9, 2018; previously published online November 9, 2018

Abstract: The increase of spatial and temporal resolution for Earth observation (EO) is the ultimate driver for science and societal applications. However, the state-of-the-art EO missions like DigitalGlobe's Worldview-3, are very costly. Moreover, this system has a high mass of 2800 kg and limited swath width of about 15 km which limits the temporal resolution. In this article, we present the status of the deployable space telescope (DST) project, which has been running for 6 years now at the Delft University of Technology, as a cutting-edge solution to solve this issue. Deployable optics have the potential of revolutionising the field of high resolution EO. By splitting up the primary mirror (M1) of a telescope into deployable segments and placing the secondary mirror (M2) on a deployable boom, the launch volume of a telescope can be reduced by a factor of 4 or more, allowing for much lower launch costs. This allows for larger EO constellations, providing image data with a much better revisit time than existing solutions. The DST specification baseline, based on Wordview-3, aims to provide images with a ground resolution of 25 cm (panchromatic 450–650 nm) from an orbital altitude of 500 km. In this paper, the current status of the optical, thermo-mechanical, and active optics systems design are described. The concurrent design approach combined with a strict bottom-up and top-down compliant systems engineering approach show that the DST is a healthy system concept.

***Corresponding author: Hans Kuiper,** Space Instrumentation and ADCS Chair, Space Engineering, Faculty of Aerospace Engineering, Delft University of Technology, Kluyverweg 1, 2629HS Delft, The Netherlands, e-mail: j.m.kuiper@tudelft.nl
Dennis Dolkens and Victor Villalba Corbacho: Delft University of Technology, Kluyverweg 1, 2629HS Delft, The Netherlands

www.degruyter.com/aot

Keywords: concurrent systems engineering; cutting-edge solution; deployable optics; planetary observation; space telescope.

1 Introduction

High resolution Earth observation (EO) is used more and more for a broad range of applications, ranging from high precision farming and environmental monitoring to defence and security.

High resolution EO images are currently provided by systems like DigitalGlobe's Worldview-3 [1]. This system can deliver images with a ground sampling distance (GSD) of 31 cm from an orbital altitude of 622 km, but this comes at a high cost. With a mass of 2800 kg and a mission cost of 600 M$, the system is very heavy and expensive, leading to high image costs. Furthermore, the swath of Worldview-3 is small, approximately 15 km, allowing only narrow strips of land to be observed on each overpass. As such for many regions on Earth, fresh image data is often unavailable.

Deployable optics have the potential of revolutionising the field of high resolution EO. By splitting up the primary mirror (M1) of a telescope into deployable segments and placing the secondary mirror (M2) on a deployable boom, the launch volume of a telescope can be reduced by a factor of 4 or more, allowing for much lower launch costs. The reduction in costs would allow for larger EO constellations, providing image data with a much better revisit time than existing solutions.

The deployable space telescope (DST) has been under development for 6 years at Delft University of Technology. The concept aims to provide a ground resolution of 25 cm from an orbital altitude of 500 km. In this paper, the current status of the optical design, thermo-mechanical design, and active optics systems are described. The project is organised as a team of MSc students, two PhD students as authors of this paper, and a senior systems engineer as manager (second author) in

close corporation with Airbus Defence and Space Leiden, TNO Space and ESA.

2 Optical design

In Table 1, the key design specifications of the DST are listed. These were derived from the specifications of Worldview-3 [1], which is taken as a reference point in the development of the system. The properties in the table are chosen such that the DST can compete with this system in terms of ground sampling distance and signal-to-noise ratio.

To meet these requirements, several optical design options have been considered. In an earlier trade-off [2], the optical concept selection was limited to fully reflective designs, so that chromatic aberrations can be avoided. Chromatic aberrations can result not only in reduced image quality and smaller bandwidths but will also complicate the design of the active optics system.

Table 1: Design specifications of the deployable telescope.

Aperture diameter	1.5 m
Focal length	11 m
Orbital altitude	500 km
Swath width	5 km
Cross-track field of view	0.6°
GSD	
Panchromatic (450–650 nm)	25 cm
Blue (450–510 nm)	100 cm
Green (520–580 nm)	100 cm
Yellow (580–630 nm)	100 cm
Red (630–700 nm)	100 cm

In the concept study, two types of telescopes were selected as the most promising to form the basis for the DST, namely the full-field Korsch and the annular-field Korsch [3, 4]. Compared to the first one, the annular-field Korsch supports a larger cross-track field of view (FOV), has a reduced alignment sensitivity of the M2 mirror, and an accessible exit pupil. The latter is beneficial for two reasons; first, a deformable mirror (DM) can be placed in the exit pupil plane, allowing for correction of aberrations resulting from M1 mirror deformations. Second, baffles can be placed around the exit pupil for straylight rejection. The total length of the annular Korsch design is longer, but when the secondary mirror is folded down, the difference in stowed volume between the two designs is minimal.

In Figure 1, the DST design and aperture shape are shown. The aperture consists of four rectangular segments that are tapered in the centre. The shape and number of segments was the result of a trade-off in which the modulation transfer function (MTF) at Nyquist, deployed aperture area, stowed volume and system complexity were taken into account.

2.1 The annular-field Korsch optical baseline design of the DST

The location of the DM and focal plane array (FPA) have been indicated in Figure 1. The four deployable segments (blue) of the primary mirror (M1) are shown whilst the black lines indicate the stowed position of the segments and the position of the tertiary mirror (M3).

The optimization of the telescope was performed in Matlab using the in-house developed toolbox FORTA (Fast Optical Raytrace Application) [5] for the analysis of

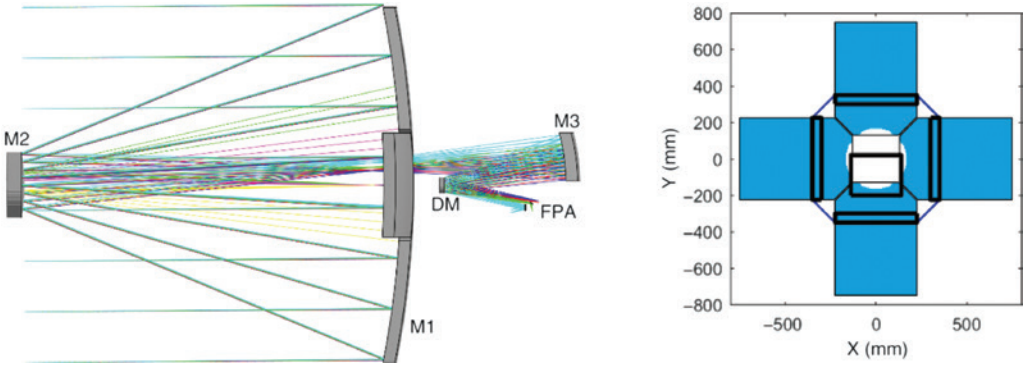

Figure 1: The annular-Field Korsch optical baseline design of the DST. The location of the DM and FPA have been indicated in the figure. The four deployable segments (blue) of the primary mirror (M1) are shown whilst the black lines indicate the stowed position of the segments and the position of the tertiary mirror (M3).

segmented telescope systems. An automatic optimisation routine was developed not only to design a system with excellent nominal performance, but also to maintain this level of performance when the system is subjected to deployment errors and instabilities. Throughout the DST design, a concurrent design philosophy was employed. As much as possible, the optical, mechanical, and active optics system designs were performed in parallel. Thus, early outcomes of the mechanical design process and active optics system design were incorporated in the optimisation of the DST considering:

Optical performance: the system was optimised to reach a diffraction limited performance across the complete FOV with distortions smaller than 1%. To improve the performance in the edges of the FOV, as well as limit the distortions, a freeform tertiary mirror (M3) was selected.

Mechanical constraints: a clearance of at least 15 mm between the beam and the DM was enforced to ensure that there is enough space to allow integration of most types of DMs. In addition, the volume available for the optical system behind M1 was kept small enough to enable the M1 mirror elements to be folded down alongside the instrument bus during launch.

Sensitivity to instabilities: during the imaging process, the telescope will be subjected to micro-vibrations, originating from the attitude determination and control system (ADCS) and other moving systems on board the spacecraft. Deployable structures, and in particular, the boom supporting M2 are sensitive to these vibrations. As such, the effect of instabilities on the optical performance was studied.

Effectiveness of active optics: in the design of the in-orbit correction system, it was found that field-dependent aberrations were the biggest driver in limiting the extent to which active optics can correct the wavefront across the entire FOV. While on-axis aberrations can be corrected using a DM in the exit pupil plane, wavefront errors for off-axis fields resulting from misalignments of the secondary and tertiary mirror cannot be fully corrected. A preliminary model of the active optics system was used to evaluate the susceptibility of a candidate design to field dependent aberrations.

In the mechanical design of the secondary mirror support structure, it was observed that the long boom lengths complicate the design. A longer boom is more susceptible to vibrations, and also imposes a requirement on the deployment ratio of it. Moreover, a short boom length results in lower F#s of the M1 and M2 mirrors, which leads to tighter alignment tolerances for these elements. Therefore, the effect of changing the length of the deployable boom was thoroughly studied.

Using paraxial optics, a number of starting points were calculated with boom lengths between 900 and 1800 mm. Each of these designs was optimised using a Nelder-Mead simplex method [6]. Subsequently, for each of the candidate designs, two Monte Carlo analyses are performed: one to assess the sensitivity to instabilities occurring during imaging operations, and another to assess the degree to which deployment errors can be corrected across the entire FOV. In both Monte Carlo analyses, the budgets given in Table 2 were used to generate random errors on the position and tilt of each element. In the analysis for the effect of instabilities, the magnitude of the displacements for the M2 mirror were scaled by the factor $f(L)$ to be calculated with Eq. (1):

$$f(L) = \frac{8M_{M2}L^3 + 3\dot{m}_{\text{boom}}L^4}{8M_{M2}L_{\text{ref}}^3 + 3\dot{m}_{\text{boom}}L_{\text{ref}}^4} \tag{1}$$

where L is the length of the boom, M_{M2} is the mass of the secondary mirror and $\dot{m}_{\text{boom}}$ is the mass per unit length of the boom. The reference boom length L_{ref}, for which the budgets were originally derived is 1.6 m. This gives an advantage to systems with a shorter boom lengths, partly compensating the increased alignment sensitivity of the M2 and the M1 segments. The equation was derived by combining beam deflection equations for a point load and a distributed load [8].

The deployment tolerances are in part compensated by the active optics system consisting of 3 degrees of freedom (DOF) control underneath the primary mirror segment (piston, tip, and tilt) and a DM in the exit pupil plane.

In Figure 2, the results of the optimisation and analysis process are shown. The left panel shows the Strehl ratio of the nominal design; averaged across the FOV, the level attained at 90% of the FOV and the minimum value seen in the corners of the FOV. In the right panel, the average

Table 2: Top-down tolerance budgets [7].

Element	Position (µm)			Tilt (µrad)		
	X	Y	Z	X	Y	Z
Deployment tolerances						
M1	2	2	2	2	4	50
M2	15	15	10	100	100	100
M3	4	4	4	10	10	50
Stability budget						
M1	$5*10^{-3}$	$5*10^{-3}$	$5*10^{-3}$	$2.5*10^{-3}$	$1*10^{-2}$	$5*10^{-1}$
M2	1	1	$5*10^{-1}$	1.5	1.5	3
M3	$2.5*10^{-2}$	$2.5*10^{-2}$	$2.5*10^{-2}$	$2.5*10^{-1}$	$2.5*10^{-1}$	1.25

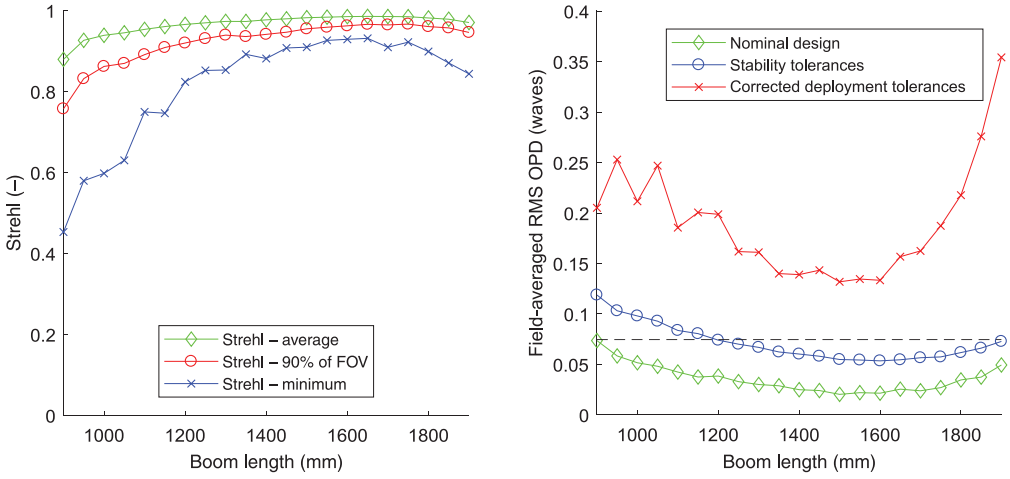

Figure 2: Plots showing the secondary mirror (M2) boom length optimisation. The left plot shows the Strehl ratio as optimisation objective whilst the right plot the field averaged RMS OPD as optimisation objective.

root mean square (RMS) optical path difference (OPD) is given for each design. The DST system performance is shown at nominal conditions, but also when subjected to stability and deployment tolerances.

2.2 Plots showing the M2 boom length optimisation

The left plot shows the Strehl ratio as optimisation objective whilst the right plot the field averaged RMS OPD as optimisation objective.

In the charts, it can be seen that for a boom length of 1600 mm, the nominal optical performance across the FOV is best. For the complete FOV, the Strehl ratio is well above the 0.8 diffraction limit. When stability tolerances are taken into account, the design maintains a lead over systems with shorter boom lengths, despite the tighter stability budgets modelled for these systems. The stability advantages of a shorter boom are largely lost due to the increased alignment sensitivity of the primary mirror segments.

When corrected deployment tolerances are considered, it can be seen that significant degradations in performance are observed. This degradation is the result of field dependent aberrations that remain when the DM is used to correct aberrations for a single field. It can be seen that the best performance is obtained for a system with a boom length of 1500 mm. For longer boom lengths, the average performance across the field drops rapidly. For longer boom lengths, the size of the exit pupil, and hence the DM, becomes smaller due to a reduced focal length of the M3 mirror. By the reduction in size, the DM becomes less effective leading to stronger field dependent aberrations.

3 Thermo-mechanical design

The mechanical assembly of the DST guarantees the functionality of the instrument after the launch and precision deployment, as well as its thermo-mechanical stability. The misalignment budgets given in Table 2 act as drivers for the bottom-up design of the different subassemblies. The coarse alignment budget is treated as a one-off deployment precision performance, with the drift and stability budgets acting, respectively, as low and high frequency stability margins. The required M1 calibration and actuation is controlled by a wave front error algorithm.

The optical design implied a parabolic M1 shape. Taking M1 mass, its resistance to gravity sag, and fundamental Eigen-frequencies into account, the mirror was chosen to incorporate triangular hollow pockets at the bottom, within a flat bottom. The design is optimised for mass and gravity whilst the latter drives the ground-testing. SiC was chosen as the mirror material due to its high strength, low coefficient of linear thermal expansion (CTE) in the operating temperature range, and relatively high thermal conductivity. The DST system design is in a recursive system optimisation where subsystems, material choices, etc., are in a continuous flow of a system of systems optimisation. Optical, thermal, and cost are the primary drivers of the SiC choice which may change. The size and geometry of the pockets and the location of the whiffle nodes were determined by optimising for gravity and thermal load conditions. The maximum modelled

deformation was 58 nm for gravity loading. Thermal deformation of the mirror was 290 nm for a thermal load driven by Albedo alone. That is, steady state radiative equilibrium between the mirrors and Earth with an ideal baffle [9].

Deployment precision, thermal drift, and vibration stability requirements can be met by the deployment mechanism. The required deployment precision being less stringent than the required phasing precision. A novel concept with four M1 segments, very different from the earlier considered options (with three M1 mirror segments), was developed which benefits the M2 deployment mechanism as well. In order to reduce the potential modes of failure, the actual design presents a combined deployment mechanism for the primary and secondary mirrors. A series of ribbons connecting the M1 and M2 deployment mechanisms will improve the structural stiffness and vibration stability of the M2 deployment mechanism, while applying the required pre-load to the M1 deployment mechanism to fall into a high precision kinematic interface. Athermalisation is the practice of making an opto-mechanical assembly insensitive to changes in bulk temperature. The three classical methods of athermalisation, namely passive, passively compensated, and actively compensated [10], are applied throughout the design.

First-order analysis has shown that this design is feasible to meet all requirements, except for the one defining the mass budget [11]. The mechanism is to be powered by four tape spring hinges present on the booms holding the secondary mirror. Each boom has two rectangular cross-section ribbons attached, connecting it to the primary mirror's support frame. As these booms extend, they pull the support frame, which in turn holds the fine actuation system and the primary mirror itself. This support frame is also equipped with a winch mechanism that releases and retracts the ribbon during the deployment sequence, keeping appropriate tension on the ribbons at all times. This has the additional advantage of providing damping for the deployment end-shock. As it is pulled, the M1 support frame falls into a kinematic interface built in the space between the mirror and the instrument housing. This kinematic interface provides a repeatable 6 DOFs constraint to the motion of the frame, provided there is sufficient preload. The latter is again provided by tightening the ribbon [12]. Figure 3 shows the deployable structure with the lines pulling the primary mirror segments in place.

Top view of the M1 subsystem in deployed configuration. The green areas mark where the lines can extend through without blocking a part of the aperture.

The original proposal of the fine actuation mechanism includes three actuators per mirror which connect to a whiffletree (triangular support elements) each. These in turn connect to a node of the mirror pockets. The whiffletrees are mechanisms that can distribute mechanical loads in the system evenly and are able to reduce stresses in the mirror due to force transmission. Each whiffletree is actuated for calibration purposes with typical values given in Table 3. These values were derived from a rigid body kinematics simulation assuming a 10 nm actuator similar to the fine actuation stage of the James Webb space telescope (JWST) [13].

Render of the early M1 mirror design, including the three triangular support elements (whiffles) and calibration actuators [9] shown in Figure 4.

Table 3: Actuator calibration precision and allowable deployment error for tip, tilt, and piston correction [9].

	Tip	Tilt	Piston
Actuation precision	51 nrad	32 nrad	10 nm
Allowable deployment error	15.5 μrad	9.9 μrad	13.0 μm

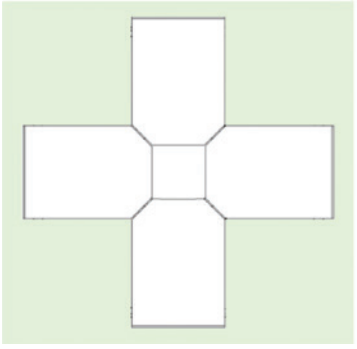

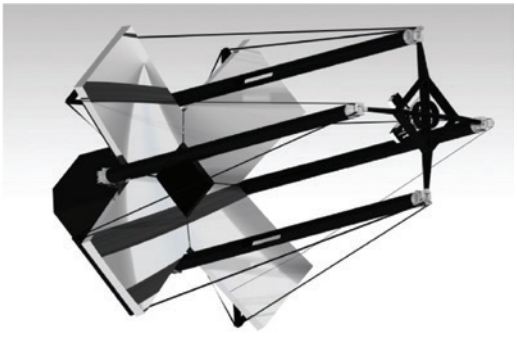

Figure 3: Top view of the M1 subsystem in deployed configuration. The green areas mark where the lines can extend through without blocking a part of the aperture.

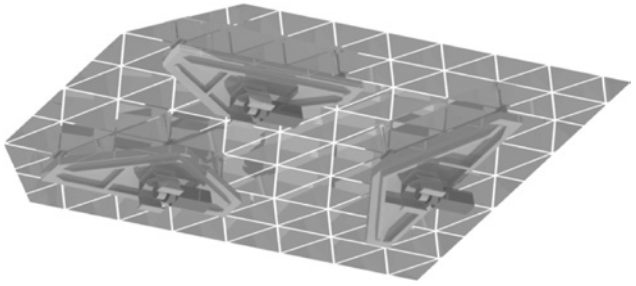

Figure 4: Render of the early M1 mirror design, including the three triangular support elements (whiffles) and calibration actuators [9].

In addition to actuating the mirrors, the fine actuation mechanism keeps them in place during the launch, providing the main load path between the mirror and the instrument housing. An uncertainty in the ability of the original concept to do this, and the fact that an additional athermalisation strategy of the support frame is needed, has driven a new concept of actuator which is still being examined.

In this new concept, each actuation system has four piezoelectric stacks coupled flexure joints which drive an intermediate plate. This intermediate plate is in turn exactly constrained by means of a hexapod mount to the back of the mirror. In principle it would be possible to actuate the intermediate plate with three actuators. Four are chosen to establish a Wheatstone bridge between strain gauges placed at the piezoelectric stacks on opposite sides of the mechanism. This helps negate the thermal effects which distort the response of the stack to control signals [14].

Other than the tape spring middle hinge that every boom has, there also need to be hinged at both ends of the boom so that they can rotate over the attachment points to the instrument housing and the M2 spider. The current concept incorporates X_R type compliant rolling element (CORE) hinges. This type of hinge is found in precision applications in the medical industry [15] due to their low hysteresis, lack of backlash, and good load carrying capacity. To the best of our knowledge, this type of hinge has not been proposed for space-based applications. The M2 spider holds the secondary mirror by means of a hexapod mount as a means of athermalisation. This athermalisation is achieved by letting the hexapod thermally expand, which moves the M2 towards M1, whilst thermal expansion of the booms move it away from it. This can be achieved either by controlling the heat rejection at the top of the spider or by actively heating it with an electrical resistance. In either case, the total heat needed to compensate for the temperature swing of the boom over an orbit is 120 J, but this method will require further investigation.

The entire assembly is to be covered by an inflatable baffle. Its purpose is two-fold: to provide stray light attenuation, and to block out the influence of sunlight on the thermal behaviour of the structure. The current concept (not shown in the figure) features an inflatable aluminium frame attached to multi-layer-blankets (MLI) blankets. The frame is inflated through the use of a nitrogen gas generator to sufficient pressure to cause yield of some of its elements. Once yielded, these elements can provide the baffle with a sufficient degree of stiffness. The gas is then vented to space. The external layer of the baffle is a flat reflector, whilst the internal layer is a super-black coating.

The complete instrument has an estimated mass that is equal to 130 kg within a stowed volume of 0.65 m^3. This figure does not include the spacecraft bus which is needed to be provided with power, communications, computing, and attitude and orbital control systems (AOCS).

4 Active optics

When all the optical elements are deployed to their intended position and maintain their intended shape, the telescope can reach a diffraction limited image quality across the complete FOV. During the launch, the telescope will be subjected to heavy loads, shocks, and random vibrations, which will ever so slightly change the position of optical components. Furthermore, deployment mechanisms have a limited precision, leading to an additional uncertainty in the deployed position of the optical elements. Finally, the telescope will be operating in a very dynamic environment, with continuously changing thermal conditions as the telescope goes in and out of eclipse. Given that mirror segments must be phased with a precision of just 10 nm to achieve a diffraction-limited performance, an active in-orbit calibration system is indispensable to be able to achieve the optimal performance. The active optics strategy is shown in Figure 5.

To correct misalignments, the telescope will have actuators underneath the primary mirror segments that can co-align and co-phase the segments. In addition, a DM in the exit pupil plane can correct higher-order aberrations as well as compensate errors occurring due to misalignments of the secondary and tertiary mirrors.

Active optics are of critical importance to ensure that the telescope can meet its performance targets after deployment of the M1 segments and the M2 boom. Throughout this process, the telescope will only make use

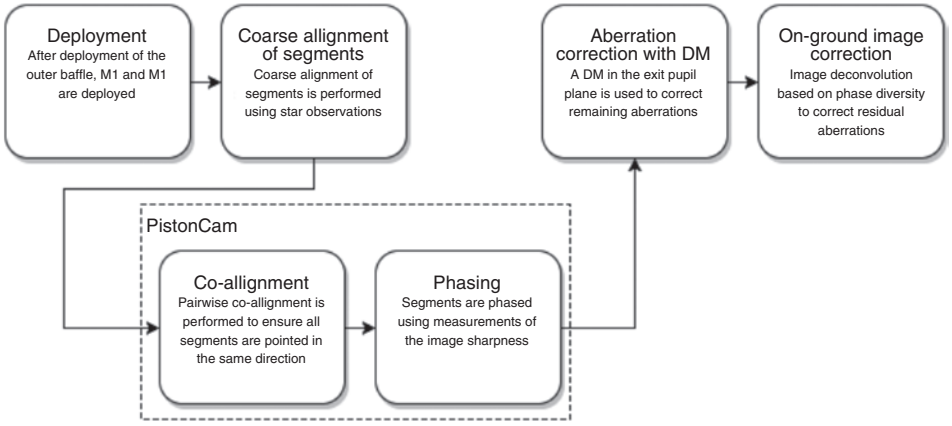

Figure 5: Active optics strategy.

of extended scenes, to ensure that the telescope can be calibrated while it remains pointed at the Earth.

In the flowchart in Figure 1, the active optics strategy is laid out. The first task of the system is to ensure that all segments are pointed into the same direction (co-alignment). After this, the segments are brought into phase and their position and orientation are fine-tuned. If acceptable segment alignment and phasing are achieved, the remaining aberrations can be corrected using a continuous DM placed in the exit pupil plane.

4.1 PistonCam

At the heart of the active optics system lies PistonCam, a novel phasing sensor. The sensor is placed in the intermediate image of the telescope, and as such, its wavefront is only affected by the primary and secondary mirrors. Relative piston and tip/tilt errors are therefore better isolated from errors occurring due to elements further down the optical path, such as the freeform tertiary mirror and the DM. Furthermore, around the intermediate image, ample space is available for this sensor, whereas the space near the focal plane is much more restricted due to the presence of detectors and read-out electronics. In Figure 6, the optical components of PistonCam are shown.

The sensor consists of the following components:

Corrector and collimator: the image quality at the intermediate image of the telescope is not a driver in the optimisation of the telescope. Therefore, the wavefront at this location is highly aberrated. An achromatic four element corrector and collimator was designed to collimate the light, create a conjugate pupil image and correct aberrations for the nominal optical design.

Pupil mask: in the conjugate pupil plane, a pupil mask is placed which ensures that light can only pass if it originates from a region where two segments meet. For this telescope design, the pupil mask shall contain

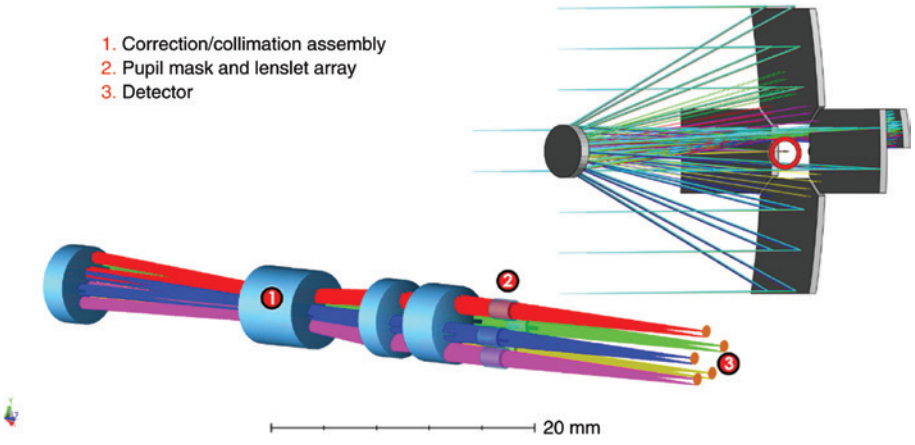

Figure 6: Optical design of PistonCam.

four openings for each boundary zone, as well as a fifth opening which is unaffected by any piston errors and therefore serves as a reference.

Lenslets: directly behind the pupil mask, a lenslets will be positioned that focus the light from each opening into a separate image on the detector.

Detector: a detector is placed in the focus of the lenslets capturing each of the images.

Conceptually, the sensor is similar to the Shack-Hartmann sensor used on, for instance, the Keck telescope. The sensor on Keck can phase the telescope through measuring a coherence parameter (using the broadband phasing algorithm [16]) or through analysis of the point spread function (using the narrow band phasing algorithm [17]). PistonCam, however, works with broadband extended scenes and can phase the telescope through iterative optimising the sharpness criterion of each sub-image.

Various definitions of a sharpness criterion apply, the most common one is given by Eq. (2):

$$S = \int dx\, dy\, I^2(x, y) \tag{2}$$

where I is the intensity and x and y are image co-ordinates. It can be shown [18] that the equation reaches a maximum in the absence of wavefront aberrations in the optical system. Calculating the criterion is not computationally intensive, making it suitable for closed-loop correction strategies.

Throughout the calibration process, the telescope must track a ground scene, such that there are minimal changes in the object throughout the process. Minimising the number of iterations is therefore one of the main priorities in the tuning of the optimisation scheme. A variety of optimisation schemes, with mixed success. The large number of local maxima that are encountered when searching for the optimal piston position complicates the process. The following approach was defined that can robustly find the global maximum in image quality for all four piston camera images. The approach includes the following steps:

1. Focus M1 for reference channel: first of all, one of the M1 segments is refocussed such that the sharpness criterion in this channel is optimal. This step ensures that the reference image reflects the maximum sharpness that can be achieved in the other channels. The refocussed mirror segment will now serve as the reference to which the other segments will be aligned.
2. Co-align segments: using a downhill Nelder-Mead simplex method, the tilts along the x- and y-axes of the segments are optimised. In Figure 7, the convergence of this process is visualised for one of the channels. To improve the robustness of the algorithm, it is recommended to perform this process one segment at a time. When all segments are co-aligned simultaneously the optimisation tends to get stuck in a local minima.
3. Scan segments to find piston errors: in this step, two segments are scanned through the actuation range and the sharpness is recorded. In Figure 8, the variation of image sharpness with the z-position of two of the segments is plotted. The sharpness co-efficient is normalised with respect to the sharpness observed in the reference channel. As the sharpness in this channel is also affected by aberrations like defocus and astigmatism, the normalised sharpness in the PistonCam channels may exceed 1. The highest peaks in the charts correspond with the position where two adjacent segments are in phase.
4. Correct segment positions and tilts: based on the peaks in the charts on Figure 8, the wavefront in each of the channels can be approximated. The wavefront is approximated by assuming that it is purely influenced by the differential piston error between the two

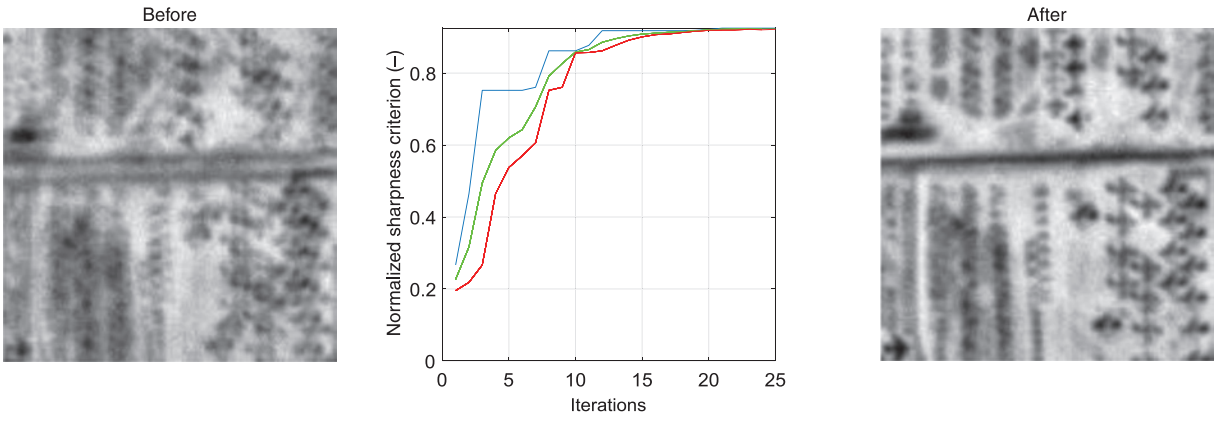

Figure 7: Co-alignment using a Nelder-Mead simplex method. The blue, green, and red lines in the centre figure respectively indicate the metric value for the best, average, and worst vertices of the simplex.

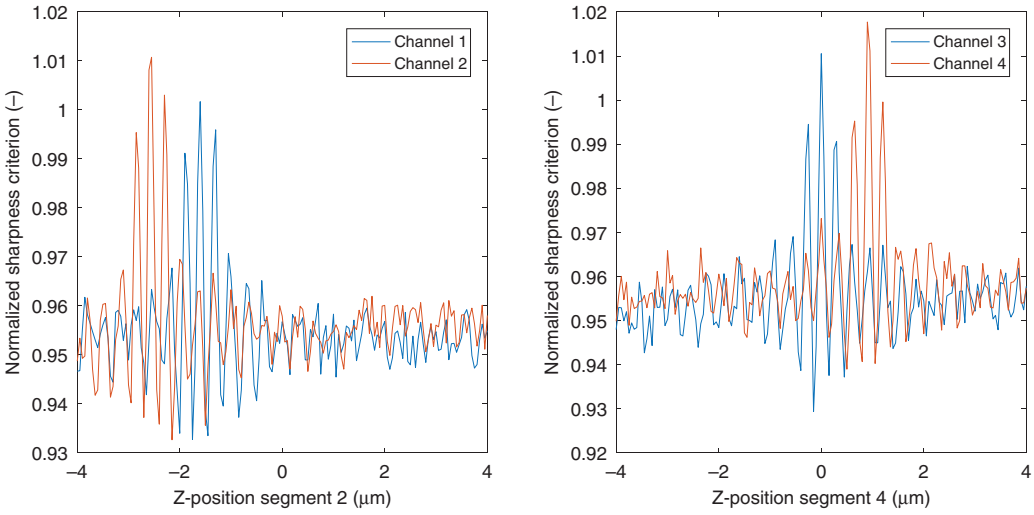

Figure 8: Sharpness variation for z-position of segments (low contrast case).

segments, as no information is available about any other aberrations that may be present in each PistonCam channel. The estimated wavefronts are fed into a linearised model of the telescope. This model is solved to find a combination of segment piston and tip/tilt actuations that minimises the wavefront.

5. Finetune the position and tilt of each segment: for large errors, correcting the piston errors in a single step may introduce tilt errors in the wavefront. For mild errors, these can be corrected with a final optimisation of all DOF the segments. For large errors, this process will likely result in poor sharpness in one of the PistonCam channels. When this is detected, the process should be restarted from step 2.
6. Correct remaining aberrations with a DM: using a DM placed in a conjugate pupil plane, the remaining aberrations can be corrected. A continuous DM can be used, as PistonCam has removed discontinuities in the wavefront. In the next section, the aberration correction process is described in more detail.

In Figure 9, typical wavefront maps at three stages of the calibration process are shown. The panel on the left shows the initial wavefront. Large piston and tilt aberrations are present, resulting in a total peak-to-valley (P-V) wavefront error larger than 10 waves (for a reference wavelength of 450 nm). In each Pistoncam channel (indicated by the black boxes) differential piston errors can be observed. After the phasing process, the wavefront in the centre figure is obtained. The P-V of the wavefront aberrations has been reduced by a factor 3, but large aberrations remain. However, differential piston errors are no longer present in each channel. From this point onwards, the wavefront is considered to be continuous and can be corrected with a DM. In Section 5, the correction with a DM will be described in more detail.

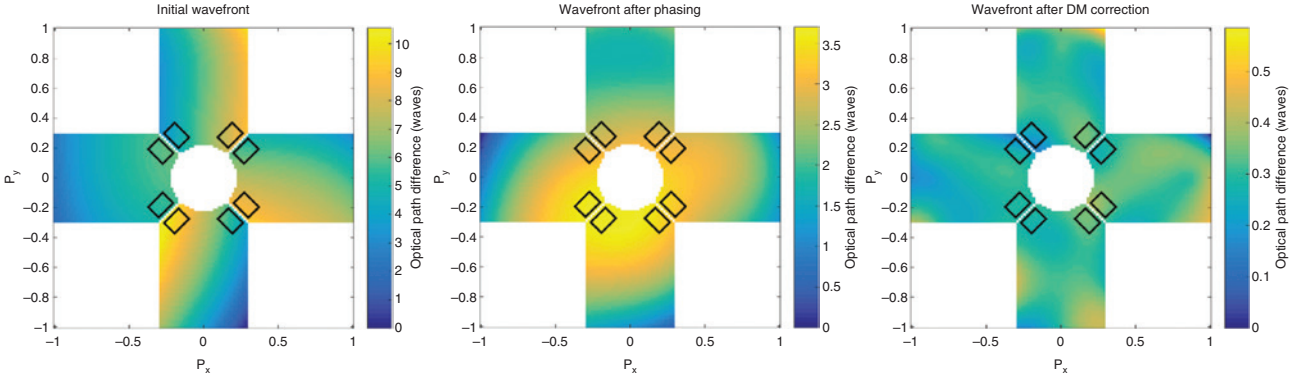

Figure 9: Initial wavefront after deployment, the wavefront after the phasing process, and the final wavefront obtained after the residual wavefront has been corrected with a DM. The areas of the pupil sampled by PistonCam are indicated by the black boxes.

5 Aberration correction with a DM

The co-alignment and phasing process described in the previous section does not fully correct wavefront aberrations; it only optimises the wavefront in segment boundary regions. It ensures, however, that the wave-front can be considered continuous in the remainder of the calibration process. The remaining wavefront error is dominated by low order aberrations, such as focus, spherical aberrations, and astigmatism. The aberrations are mainly the result of misalignment and displacement of the secondary mirror. Once these low order aberrations have been corrected, higher order aberrations remain, caused mainly by deformations of the primary mirror segments. Based on extensive Monte Carlo analyses it was determined that up to 36 Zernike modes (Noll's numbering scheme) must be corrected to sufficiently address all aberrations.

To correct the remaining aberrations, several techniques can be used. In the DST, two aberration correction techniques have been considered. First, the use of an extended scene Shack-Hartmann sensor was considered. This type of sensor provides a direct estimate of the slope of the wavefront and as such can correct the wavefront in only a few iterations, depending on the contrast of the scene, signal-to-noise ratio and mechanical characteristics of the DM. The main downside of the method is that extra optical hardware is required; the sensor needs to be placed in a collimated beam in the exit pupil plane. Given the compact instrument design, there is very little space available for the pupil re-imaging optics. Furthermore, to calculate the wavefront slopes, computationally intensive cross-correlation computations are needed. Second, the wavefront observed at the Shack-Hartmann sensor is affected by non-common path errors, resulting amongst others from misalignments in the pupil re-imaging optics.

An alternative of using a dedicated wavefront sensor is to iteratively optimise the image sharpness observed at the detector plane. Various optimisation algorithms can be used to optimise the shape of the DM. Within the deployable telescope project, the Nelder-Mead simplex method and a parallel stochastic gradient descent method are being considered. In simulations, the Nelder-Mead simplex methods converges faster and to higher sharpness values than the parallel stochastic gradient method, but the method is more vulnerable to hysteresis of the DM actuators.

In Figure 10, the results of a simulation of the sharpness optimisation process is shown. In this simulation, the Nelder-Mead simplex method is used to optimise the shape of the DM. As can be seen, after 1000 iterations, the image quality has improved dramatically. In Figure 11, the MTF of the telescope is shown before and after the optimisation process. For the central field, the MTF performance is virtually diffraction limited. The MTF in the corner of the FOV (0.3°), cannot reach its design levels, falling short of the diffraction limit. Field dependent aberrations resulting from displacements of the secondary and tertiary mirror cannot be fully corrected with a DM in the exit pupil plane. Addressing these aberrations is a subject of future research and beyond the scope of this paper.

An advantage of this wavefront-sensorless approach is that limited extra hardware is required. A single array detector can be used to evaluate the image sharpness at the image plane. In addition, the approach requires less calibration since the wavefront affecting the sharpness at the main TDI (Delft, The Netherlands) detectors and the wavefront at the calibration sensor is the same, with the exception of small field dependent aberrations. Furthermore, the evaluation of the sharpness criterion at the image plane is computationally inexpensive. The main downside of this approach is that the satellite must remain pointed at a static ground scene throughout this process. To circumvent this problem, a method is developed which

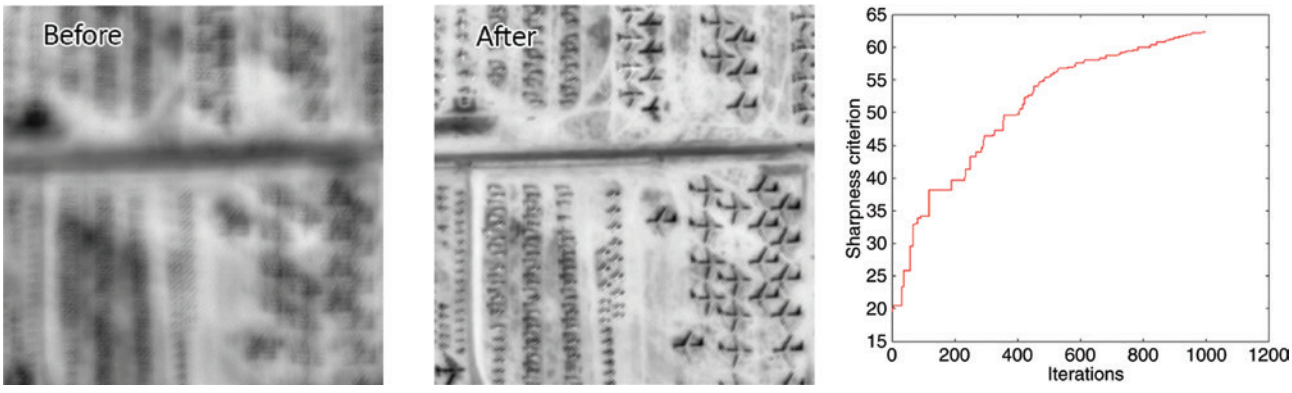

Figure 10: Before and after sharpness correction with a DM [5].

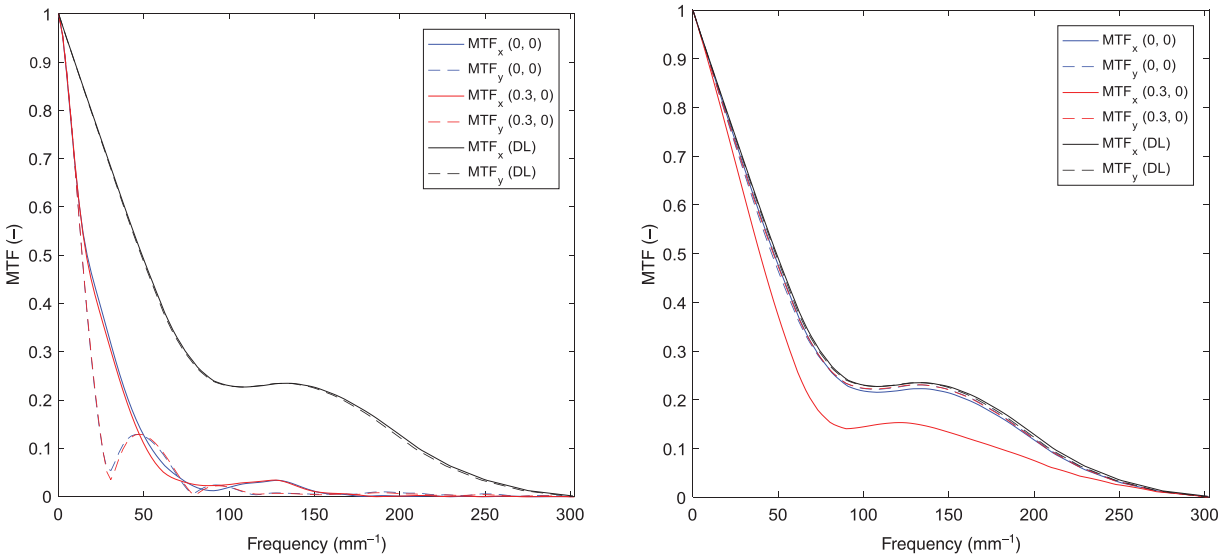

Figure 11: Typical MTF performance after step 2 (left) and after step 6 (right). The nominal optical performance is diffraction limited for the complete FOV (indicated by the black curves).

uses two parallel TDI line-scan detectors in the image plane, rather than a single array detector. As the satellite flies across a ground scene, the scene will pass through the FOV of the first detector and the image sharpness is recorded. Before the scene passes into the FOV of the second detector, the position of the DM is adjusted. The effect of this change can subsequently be observed using the secondary detector allowing for an estimation of the gradient and the calculation of a new DM position. Simulations of this method show promising results and will be further described in future publications.

6 Conclusions

The status of the DST project, which has been running for 6 years now at the Delft University of Technology, as a cutting-edge solution shows a healthy status.

The DST specification baseline, biased on Worldview-3, aims to provide with a ground resolution of 25 cm (panchromatic 450–650 nm) from an orbital altitude of 500 km. In this paper, the current status of the optical, thermo-mechanical and active optics systems design is described. The concurrent design approach combined with a strict bottom-up and top-down compliant systems engineering approach show that the DST is a healthy system concept.

Acknowledgements: We are grateful to a series of Master's students who made these results possible. Furthermore, the Dutch HTSM TKI funding and ESA's NPI funding made it possible to attract the PhD students being two of the three authors of this article.

References

[1] Digital Globe. Worldview 3, Above + Beyond. (2014). Available at: http://worldview3.digitalglobe.com/. (Accessed: 22nd November 2014).
[2] D. Dolkens, in 'A Deployable Telescope for Sub-meter resolution from MicroSatellite Platforms'. (Delft University of Technology, 2015). https://repository.tudelft.nl/islandora/object/uuid%3A8f73b31c-4306-4b44-9937-3b4d23a4a53f?
[3] M. Lampton and M. Sholl, in 'Comparison of On-axis Three-Mirror-Anastigmat Telescopes'. 66870S (2007). DOI:10.1117/12.732527.
[4] D. Korsch, Appl. Opt. 2, 2074–2077 (1977).
[5] D. Dolkens and H. Kuiper, in 'Design and End-to-End Modelling of a Deployable Telescope'. International Conference on Space Optics 18, 21–28 (2016).
[6] J. A. Nelder and R. Mead, Comput. J. 7, 308–313 (1965).
[7] D. Dolkens, J. M. Kuiper, B. T. de Goeij and E. K. A. Gill, in 'Design and Optimization of a Deployable Telescope for Earth Observation'. Pre-print (2018).
[8] R. C. Hibbeler, in 'Statics and Mechanics of Materials, in SI units'. (Pearson Education, London, UK, 2011).
[9] B. T. van Putten, in 'Desigh of the Deployment Mechanism for the Primary Mirror Elements of a Deployable Space Telescope'. (Delft University of Technology, 2017). https://repository.tudelft.nl/islandora/object/uuid%3A3c87afd7-5275-4c15-96f0-3d77fde517b1.
[10] P. Y. Bely, in 'The Design and Construction of Large Optical Telescopes'. (Springer, Berlin, Germany, 2003).
[11] A. Krikken, in 'Design of the Secondary Mirror Support Structure for the Deployable Space Telescope'. (Delft University of

Technology, 2018). https://repository.tudelft.nl/islandora/object/uuid%3A9252841c-7a7c-4c8c-a418-9127b724d364?
[12] M. Corvers, in 'Design of the Deployment Mechanism for the Primary Mirror of a Deployable Space Telescope'. (Delft University of Technology, 2018). https://repository.tudelft.nl/islandora/object/uuid%3Aa8bbf4a1-1222-41e0-96f5-94aa33a93d45.
[13] R. M. Warden, Cryogenic Nano-Actuator for JWST. in 38th Aerospace Mechanisms Sympsium (2006).
[14] S. Pepper, in 'Deployable Space Telescope: Design & Feasibility Assessment of the Primary Mirror Active Optics Mechanism (draft)'. (Delft University Technology, 2018).
[15] A. Jeanneau, J. Herder, T. Laliberté and C. Gosselin, Proc. ASME Des. Eng. Tech. Conf. 2 A, 1–9 (2004).
[16] G. Chanan, C. Ohara and M. Troy, Appl. Opt. 37, 140–155 (1998).
[17] G. Chanan, C. Ohara and M. Troy, Appl. Opt. 39, 4706–4714 (2000).
[18] R. A. Muller and A. Buffington, J. Opt. Soc. Am. 64, 1200–1210 (1974).

Dennis Dolkens
Delft University of Technology, Kluyverweg 1
2629HS Delft, The Netherlands

Dennis Dolkens is a PhD candidate in the Department Space Engineering at the Faculty Aerospace Engineering of the Delft University of Technology. He has been working on the Deployable Telescope for 6 years, first as an MSc student and after that as a part of his PhD research.

Hans Kuiper
Space Instrumentation and ADCS Chair,
Space Engineering, Faculty of Aerospace Engineering, Delft University of Technology
Kluyverweg 1, 2629HS Delft
The Netherlands
j.m.kuiper@tudelft.nl

Hans Kuiper is a senior systems engineer, senior research manager and Assistant/Professor in the department of Space Engineering at the Faculty of Aerospace Engineering of the Delft University of Technology. Before joining the TU Delft in 2008 he worked for 28 years in the Dutch high-tech industry as a senior systems engineer and research group leader within Philips Research, Dutch Space (now ADS Leiden) and ASML, respectively.

Victor Villalba Corbacho
Delft University of Technology, Kluyverweg 1
2629HS Delft, The Netherlands

Victor Villalba Corbacho is a PhD candidate in the Department of Space Engineering at the Delft University of Technology. His research interests are in space systems engineering and thermal structures for space applications.